Rigorous interpolation near tilted interfaces in 3-D finite-difference EM modelling

Daniil V. Shantsev[1] and Frank A. Maaø[2]

[1]*EMGS, I&I Technology Center, POB* 2087 *Vika,* 0125 *Oslo, Norway. E-mail: dshantsev@emgs.com*
[2]*Statoil Research Centre, Rotvoll, Arkitekt Ebbells veg* 10, 7005, *Trondheim, Norway*

SUMMARY

We present a rigorous method for interpolation of electric and magnetic fields close to an interface with a conductivity contrast. The method takes into account not only a well-known discontinuity in the normal electric field, but also discontinuity in all the normal derivatives of electric and magnetic tangential fields. The proposed method is applied to marine 3-D controlled-source electromagnetic modelling (CSEM) where sources and receivers are located close to the seafloor separating conductive seawater and resistive formation. For the finite-difference scheme based on the Yee grid, the new interpolation is demonstrated to be much more accurate than alternative methods (interpolation using nodes on one side of the interface or interpolation using nodes on both sides, but ignoring the derivative jumps). The rigorous interpolation can handle arbitrary orientation of interface with respect to the grid, which is demonstrated on a marine CSEM example with a dipping seafloor. The interpolation coefficients are computed by minimizing a misfit between values at the nearest nodes and linear expansions of the continuous field components in the coordinate system aligned with the interface. The proposed interpolation operators can handle either uniform or non-uniform grids and can be applied to interpolation for both sources and receivers.

Key words: Numerical solutions; Numerical approximations and analysis; Electrical properties; Electromagnetic theory; Marine electromagnetics.

1 INTRODUCTION

A number of electromagnetic (EM) methods for geophysical exploration use data from receivers located at the seafloor in order to extract information about the resistivity distribution in the subsurface. They include the marine controlled-source electromagnetic (CSEM) method where EM fields in the earth are generated by a powerful current source typically towed just above the seafloor, as well as marine magnetotelluric (MT) method that uses the natural EM radiation. One of the main application areas for these methods today is the hydrocarbon exploration because resistive hydrocarbon reservoirs often show up as anomalies in CSEM data (see e.g. Constable 2010; Hesthammer *et al.* 2010; Alcocer *et al.* 2013).

A major challenge for accurate modelling of EM data recorded by seafloor receivers is a sharp conductivity contrast between the conductive sea water and resistive formation. This conductivity jump leads to discontinuities in the EM fields at the interface. Namely, there appears a well-known discontinuity in the normal electric field, and an often overlooked discontinuity in the normal derivatives of tangential electric and magnetic fields. The latter is of primary importance for CSEM and MT since both methods are based mainly on measurements of the tangential components. Appropriate handling of these discontinuities is a prerequisite for an accurate 3-D EM modelling.

There exist three main approaches for modelling of EM responses: finite-difference/finite-volume, finite-element and integral equations schemes (see Avdeev 2005; Börner 2010) for reviews. In this work, we will focus on the finite-difference method—the most straightforward for discretization of the Maxwell equations and at the same time one of the most vulnerable to inaccurate handling of interfaces.

Proper account of field discontinuities at interfaces is important for both: (i) discretizing derivatives in the Maxwell equations on the finite-difference grid and (ii) performing interpolation between the grid nodes and the positions of sources and receivers. Some accurate formulations of finite-difference operators in 3-D in the presence of interfaces non-conforming to the modelling grid can be found, for example in Bauer *et al.* (2011) and Nadobny *et al.* (2003). In this work we focus on the interpolation problem where, as demonstrated below, discontinuities at interfaces may lead to even bigger inaccuracies. We shall consider an interface between two media with different conductivities, but our results can be easily generalized also to an interface between media with different dielectric permittivities.

Interpolation of electric and magnetic fields is needed whenever nodes of the finite-difference grid do not coincide with exact positions of the modelled sources and receivers. This is usually the case for measurements done with seafloor receivers since the seafloor

cannot be ideally flat and hence does not conform to the grid. Moreover, the staggered Yee grid often used for EM modelling places different field components at different nodes (see e.g. Taflove & Hagness 2005) while a CSEM receiver measures all of them at the same location. Hence, in order to find all components at a desired recording position, one always needs to interpolate the field values computed at the nearby nodes. Similarly, the interpolation is needed for the CSEM source whose trajectory through the water does not necessarily fit the grid nodes either. Smooth interpolation operators, such as, for example trilinear interpolation, do a reasonably good job as long as the conductivity varies slowly close to the interpolation site. However, near sharp conductivity contrasts, for example near the seafloor, such simple approaches are too inaccurate.

One common method to improve the interpolation accuracy is to interpolate within one medium only. Since EM receivers deployed at the seabed are located in the water, one can interpolate using only nodes in the water (see e.g. Abubakar *et al.* 2008). There exists a more powerful method—the essentially nonoscillatory interpolation—where the interpolation stencil is chosen adaptively, by minimizing oscillations in the interpolation polynomial (Wirianto *et al.* 2011). In the case of an interface, it will also choose only nodes within one medium since they represent the smoothest part of the function. Even though these approaches avoid the discontinuity issue, it comes at a cost of asymmetric interpolation stencil. The asymmetry is extreme for receiver located exactly at the seafloor: then all interpolation nodes lie higher than the receiver, i.e. interpolation is replaced by extrapolation that is inherently less accurate.

In order to use interpolation nodes on both sides of the seafloor, one should interpolate the continuous normal current density instead of discontinuous normal electric field. This approach is discussed in detail in Streich (2009) where it is also emphasized that only the secondary fields should be interpolated if the primary fields can be computed explicitly at the recording position. However, even though the normal current density is continuous, its derivative is not. The same is true for the tangential electric and magnetic fields: they also have a discontinuity in the normal derivative, in other words, their profile across the interface has a sharp bend. Disregarding this bend leads to interpolation errors.

In this work, we propose a more fundamental solution to the interpolation problem that overcomes all the above mentioned difficulties. We 'directly compute' the jumps of field derivatives at the interface using the known conductivity values on both sides of the interface. The derivative jumps are then explicitly taken into account when performing the interpolation. The proposed rigorous interpolation allows improvement in the accuracy compared to the existing schemes because (i) it uses nodes on both sides of the interface, (ii) it takes into account discontinuity of both the normal electric field and derivatives of the tangential fields and (iii) it utilizes the available information about the conductivity contrast at the interface.

We pay special attention to the important practical case of interface tilted with respect to the modelling grid. We describe an interpolation scheme that properly handles all boundary conditions at such an interface and show how the derivative discontinuities can be taken into account in that case.

Note that the CPU cost of interpolation is orders of magnitudes smaller than the cost of computing fields at the grid nodes by solving the Maxwell equations. Therefore one should always aim at using the most accurate interpolation approach. Another reason for increasingly high requirements to the accuracy of interpolation and forward CSEM modelling in general is a fast progress in the CSEM

acquisition equipment over the past years. Indeed, as the power of the source increases, while the noise in source and receiver components gets smaller (Barker *et al.* 2012), the CSEM method becomes capable of detecting targets with relative response of only a few per cent (Roth *et al.* 2013) or even resolving spatial variations of hydrocarbon saturation within a given oil reservoir (Morten *et al.* 2012).

The paper is divided into three main sections. First, we prove the concept on a simple case—a horizontal interface aligned with the grid. We provide expressions for the derivative jumps, show how they impact the interpolation coefficients and demonstrate improvement in the interpolation accuracy for two CSEM examples. Then we proceed to a general case of interface tilted with respect to the grid, present the interpolation framework, show how derivative jumps can be incorporated there and finish with numerical CSEM results for a dipping seafloor case. At the end, we provide discussion and end up with a conclusion.

2 HORIZONTAL INTERFACE

2.1 Derivative jumps

The Maxwell equations without sources, in a non-magnetic medium and with negligible displacement current read

$$\mu_0 \dot{\mathbf{H}} = -\nabla \times \mathbf{E}$$
$$\sigma \mathbf{E} = \nabla \times \mathbf{H}. \tag{1}$$

Here μ_0 is the magnetic permeability in a vacuum, while $\mathbf{E}$ and $\mathbf{H}$ are the electric and magnetic fields, respectively. The electric conductivity tensor σ is assumed to be diagonal, that is, we allow for triaxial anisotropy.

Let us consider a horizontal interface—parallel to the (x, y) plane—between two media with conductivities σ_1 and σ_2. The boundary conditions require that the normal electric field has a jump at the interface since $\sigma_{z1}E_{z1} = \sigma_{z2}E_{z2} \equiv J_z$, where J_z denotes the vertical current density. At the same time, the tangential electric and magnetic fields, E_x, E_y, H_x and H_y, are continuous across the interface. Let us now have a closer look at how their derivatives behave.

Since H_y is continuous, its time derivative, $\dot{H}_y = \partial E_x/\partial z - \partial E_z/\partial x$ should also be continuous. On the other hand, E_z has a jump across the interface and correspondingly $\partial E_z/\partial x$ also has a jump. It must be compensated by a similar jump in $\partial E_x/\partial z$, namely,

$$\frac{\partial E_{x2}}{\partial z} - \frac{\partial E_{x1}}{\partial z} = \left(\frac{1}{\sigma_{z2}} - \frac{1}{\sigma_{z1}} \right) \frac{\partial J_z}{\partial x}. \tag{2}$$

Here we have disregarded terms proportional to $\partial \sigma_z/\partial x$, that is we have assumed that the conductivity jump across the interface is much larger than variation of conductivity along the interface over a characteristic distance used to evaluate derivatives $\partial/\partial x$, that is over a size of grid cell. This equation tells us that even though the tangential field E_x is continuous across the interface, its derivative, $\partial E_x/\partial z$, experiences a jump. The jump is proportional to the jump of normal resistivities over the interface, and also proportional to the tangential derivative of the normal current density, $\partial J_z/\partial x$.

Similar results can be obtained also for the y component of electric field. From the continuity of $(\partial E_z/\partial y - \partial E_y/\partial z)$, one finds that the jump of the derivative $\partial E_y/\partial z$ is given as,

$$\frac{\partial E_{y2}}{\partial z} - \frac{\partial E_{y1}}{\partial z} = \left(\frac{1}{\sigma_{z2}} - \frac{1}{\sigma_{z1}} \right) \frac{\partial J_z}{\partial y}. \tag{3}$$

Taking into account this kind of jumps in the interpolation scheme is the central point of this paper.

The x projection of the Ampere's law (1) reads: $\sigma_x E_x = \partial H_z/\partial y - \partial H_y/\partial z$. Here H_z and hence $\partial H_z/\partial y$ are continuous, therefore a jump in $\sigma_x E_x$ across the interface must be equal and opposite in sign to the jump in $\partial H_y/\partial z$. A similar consideration can be applied to the y projection of eq. (1), which gives us the two following conditions:

$$\frac{\partial H_{y2}}{\partial z} - \frac{\partial H_{y1}}{\partial z} = (\sigma_{x1} - \sigma_{x2}) E_x$$
$$\frac{\partial H_{x2}}{\partial z} - \frac{\partial H_{x1}}{\partial z} = -(\sigma_{y1} - \sigma_{y2})E_y. \qquad (4)$$

We see that derivatives of the tangential magnetic fields are also discontinuous. Their jump is proportional to the jump of conductivities over the interface and also to the tangential electric field at the interface.

Since the normal electric field is discontinuous across the interface, it is quite common to interpolate the continuous normal current density J_z instead, and then evaluate the field as $E_z = J_z/\sigma_z$. A more careful analysis shows however that the derivative $\partial J_z/\partial z$ has a jump across the interface. Indeed, in the absence of charges, $\text{div}\mathbf{E} = 0$, and hence $\partial E_z/\partial z = -\partial E_x/\partial x - \partial E_y/\partial y$. Obviously, $\partial E_x/\partial x$ and $\partial E_y/\partial y$ are continuous across the interface, and so is $\partial E_z/\partial z$. It means that $\partial J_z/\partial z$ is discontinuous, namely,

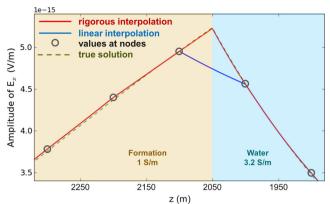$$\sigma_{z1} \frac{\partial J_{z2}}{\partial z} = \sigma_{z2} \frac{\partial J_{z1}}{\partial z}. \qquad (5)$$

We have thus seen that all continuous quantities that can be used for interpolation on both sides of the interface: the tangential fields E_x, E_y, H_x and H_y as well as the normal current density, J_z, have discontinuity in their z derivatives. The only field component that has smooth derivatives over the interface is the normal magnetic field, H_z,—but only as long as there is no discontinuity in magnetic permeability.

Note also that the derivative jump have slightly different mathematical expressions in the formulas above. For the tangential fields the jump conditions given by eqs (2), (3) and (4) define the difference' between the derivatives at the two sides of the interface. By contrast, for the normal current density J_n, the jump condition (5) defines the ratio of the derivatives.

2.2 CSEM example

Fig. 1 shows an example of field profile across the seafloor where the derivative discontinuity is seen very clearly. Here we consider a simple CSEM model consisting of air, a water layer of 2050 m and a half-space formation with resistivity of 1 Ωm. Fields are generated by a harmonic horizontal electric dipole with dipole moment of 1 Am at the frequency of 1 Hz placed 50 m above the seafloor. The inline electric field E_x is recorded at 4 km horizontal offset from the source. The dashed line shows the field profile $|E_x^{\text{true}}|$ along the vertical z axis obtained using the semi-analytical solution from Løseth & Ursin (2007). The profile exhibits a sharp bend exactly the seafloor, which means that the field derivative over z is discontinuous. The observed jump of the derivative, $\partial E_x/\partial z$, is in agreement with eq. (2) and proportional to the difference of formation and seawater resistivities.

The same CSEM problem has been solved using a 3-D finite-difference time-domain modelling code described in Maaø (2007) and Mittet (2010). The magnitude of inline field was computed at the nodes of the Yee grid that are spaced by 100 m from each

Figure 1. Magnitude of inline electric field as a function of the vertical coordinate z experiences a sharp bend at the seafloor caused by the conductivity jump. Circles indicate field values computed at the nodes of modelling grid, 100 m apart from each other. Linear interpolation between the grid nodes obviously fails to reproduce the correct field profile. However the new interpolation fits the correct field behaviour very accurately because it takes into account the derivative discontinuity at the seafloor.

other. The computed values are indicated as circles in Fig. 1. They match almost perfectly the semi-analytical solution shown by the the dashed line. To evaluate field values between the nodes, we first use a linear interpolation (blue line). It gives satisfactory results for most locations, however fails at the water—formation interface where the field derivative $\mathrm{d}E_x/\mathrm{d}z$ is discontinuous. For a receiver located exactly at the seafloor the error in the interpolated E_x is larger than 10 per cent.

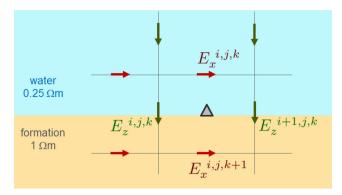Much better accuracy can be achieved by an improved interpolation scheme (red curve) where the jump in the derivative $\mathrm{d}E_x/\mathrm{d}z$ is taken into account. The interpolated field profile is therefore not just a straight line between values at the nodes: it is now given by two line segments with different slopes in the water and in the formation. The difference in the slopes is given by the jump of $\mathrm{d}E_x/\mathrm{d}z$ which is explicitly computed using eq. (2). In this way one obtains an excellent fit to the true profile of $E_x(z)$.

2.3 Interpolation coefficients

Here we shall give a very simple example showing how the interpolation coefficients can be computed if one wishes to take into account a discontinuity in the derivative of the interpolated function. We still consider a horizontal interface in the (x, y) plane and assume that it is aligned with the rectilinear grid used to discretize the Maxwell equations. In this configuration the 3-D interpolation coefficients can be obtained by multiplication of 1-D interpolation coefficients along x, y and z. In other words, one can write down the interpolated function, for example E_x, at the receiver location (x_0, y_0, z_0) as

$$E_x(x_0, y_0, z_0) = \sum_i \sum_j \sum_k c_x(i)c_y(j)c_z(k)E_x^{i,j,k}, \qquad (6)$$

where $E_x^{i,j,k}$ is the known values at the grid nodes specified by three indices i, j, k referring to x, y and z, respectively. The sum runs over relevant indices only, for example, in the popular trilinear interpolation scheme it includes just two values for i, j and k, so that the interpolation stencil covers the eight nearest nodes around the receiver. When the interface is misaligned with the grid, splitting the 3-D interpolation coefficient $c(i, j, k)$ into the product $c_x(i)c_y(j)c_z(k)$

Figure 2. Slice of the Yee grid in the (x, z) plane showing positions of E_x and E_z nodes. The triangle marks the receiver position where the E_x component needs to be interpolated. Interpolation taking into account the derivative jump at the seafloor will use not only values of the two nearest E_x nodes, but also values at the E_z nodes. Interpolation coefficients with and without the derivative jump are given in eqs (12) and (9), respectively.

is not possible, and the full derivation for this general case is given in Section 3. The horizontal interface causes derivative discontinuity in the vertical direction only, but it does not affect smooth behaviour of field components along x and y. Therefore, one may use any conventional scheme to find the interpolation coefficients c_x and c_y, and only computation of c_z needs to be modified in such a way that c_z will become dependent on the conductivity and the vertical field component, $E_z^{i,j,k}$.

Let us first find the interpolation coefficients in the absence of interface. The conventional linear interpolation is then based on the linear expansion for $E_x(z)$:

$$E_x(z) = E_x(z_0) + \frac{\partial E_x}{\partial z}(z - z_0). \quad (7)$$

It contains two unknowns, $E_x(z_0)$ and $\partial E_x / \partial z$, that can be determined by substituting here the coordinates z_k and z_{k+1} of the two nearest E_x nodes. The interpolated field at receiver is then immediately obtained as

$$E_x(x_0, y_0, z_0) = \sum_i \sum_j c_x(i) c_y(j)$$
$$\times \left[\frac{z_{k+1} - z_0}{z_{k+1} - z_k} E_x^{i,j,k} + \frac{z_0 - z_k}{z_{k+1} - z_k} E_x^{i,j,k+1} \right]. \quad (8)$$

Let us now consider a very simple case depicted in Fig. 2 which shows a slice of the Yee grid in the (x, z) plane that contains E_x and E_z nodes. The receiver is located exactly in the middle between two E_x nodes: one above and one below it, that is has the same x and y coordinates as the two E_x nodes. It means that no interpolation is required in x and y, hence, the sums over i and j in the above expression disappear, while both interpolation coefficients in z equal $1/2$. It leads to the very intuitive result that the interpolated field at receiver is a simple average of the fields at the node above and the node below,

$$E_x(x_0, y_0, z_0) = \frac{E_x^{i,j,k} + E_x^{i,j,k+1}}{2}. \quad (9)$$

In the presence of interface, the expansion (7) is not valid anymore since the derivative $\partial E_x / \partial z$ has different values in the two media. If we denote its value in medium 1 as $\partial E_{x1} / \partial z$, then the updated

linear expansion can be written down using eq. (2) as

$$E_x(z) =$$
$$E_x(z^*) + \begin{cases} \dfrac{\partial E_{x1}}{\partial z}(z - z^*), & z \in \Omega_1 \\[2ex] \left[\dfrac{\partial E_{x1}}{\partial z} + \left(\dfrac{1}{\sigma_{z2}} - \dfrac{1}{\sigma_{z1}} \right) \dfrac{\partial J_z}{\partial x} \right](z - z^*), & z \in \Omega_2, \end{cases}$$
$$(10)$$

where z^* denotes the position of interface separating medium 1 (Ω_1) and medium 2 (Ω_2). The derivative $\partial J_z / \partial x$ should be taken at the location (x_0, y_0, z^*), that is, at the projection of receiver to the interface. By substituting here coordinates z_k and z_{k+1} of the two nearest nodes, we obtain a system of two equations that can be solved to find the two unknowns: $E_x(z^*)$ and $\partial E_{x1} / \partial z$. Then the field at the receiver position is immediately found from eq. (10) as

$$E_x(x_0, y_0, z_0) = \sum_i \sum_j c_x(i) c_y(j)$$
$$\times \left[\frac{z_{k+1} - z_0}{z_{k+1} - z_k} E_x^{i,j,k} + \frac{z_0 - z_k}{z_{k+1} - z_k} E_x^{i,j,k+1} \right.$$
$$\left. - \frac{(z_{k+1} - z^*)(z_0 - z_k)}{z_{k+1} - z_k} \left(\frac{1}{\sigma_{z2}} - \frac{1}{\sigma_{z1}} \right) \frac{\partial J_z}{\partial x} \right], \quad (11)$$

where we have assumed that the receiver is located in medium 1. Note that field at the interface $E_x(z^*)$ is given by the same expression (11) if one replaces z_0 by z^*. It is interesting to compare this expression with a similar expression (8) in the absence of interface. We notice that they are identical except that now there appears an additional term which is proportional to the derivative jump at the interface. This is a very practical result since it allows one to reuse the standard interpolation expressions and take into account the presence of interface by simply adding a new term.

Let us now come back to the simple case shown in Fig. 2. Here the derivative $\partial J_z / \partial x$ at (x_0, y_0, z^*) can be evaluated using the centred finite-difference as, $\partial J_z / \partial x = (J_z^{i+1,j,k} - J_z^{i,j,k})/\Delta x$, where Δx is the Yee cell size in the x direction. Eq. (11) for the interpolated E_x at the receiver then reduces to
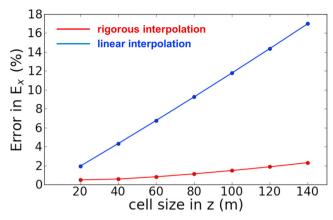
$$E_x(x_0, y_0, z_0) = \frac{E_x^{i,j,k} + E_x^{i,j,k+1}}{2}$$
$$- \frac{1}{4} \frac{\Delta z}{\Delta x} \left(\frac{1}{\sigma_{z2}} - \frac{1}{\sigma_{z1}} \right) \left(J_z^{i+1,j,k} - J_z^{i,j,k} \right). \quad (12)$$

Again we see that this expression contains the same terms as in the absence of interface, eq. (9), plus one more term proportional to the derivative jump at the interface.

Let us now get a feeling of the magnitude of the new interpolation coefficients by substituting typical conductivity values: $\sigma_{z1} = 4\,\mathrm{S\,m^{-1}}$ for the water and $\sigma_{z2} = 1\,\mathrm{S\,m^{-1}}$ for the top formation. The relation between the normal current density $J_z^{i,j,k}$ and the normal electric field $E_z^{i,j,k}$ involves the effective conductivity assigned to the $E_z^{i,j,k}$ node located exactly at the seafloor. In a finite-volume scheme it should be obtained by harmonic averaging of water and formation conductivities, that is, $\sigma_z^{i,j,k} = 2\sigma_{z1}\sigma_{z2}/(\sigma_{z1} + \sigma_{z2})$ that gives $1.6\,\mathrm{S\,m^{-1}}$. Finally, we assume equal cell sizes in x and z directions, $\Delta x = \Delta z$ and then eq. (12) becomes,

$$E_x(x_0, y_0, z_0) = 0.5 \left(E_x^{i,j,k} + E_x^{i,j,k+1} \right) - 0.3 \left(E_z^{i+1,j,k} - E_z^{i,j,k} \right), \quad (13)$$

where the first term represents the standard linear interpolation, while the term with coefficient 0.3 accounts for the derivative jump
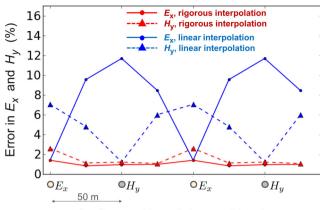
Figure 3. Error in the inline electric field recorded at the seafloor as a function of the cell size in z direction for a half-space CSEM model described in the text. The conventional linear interpolation (blue) has a first-order error which is removed when using the proposed rigorous interpolation (red).

at the interface. Note that the coefficients for the two terms are of the same order. The additional term due to the derivative jump is smaller only because the two E_z nodes enter the expression with the opposite signs and there will be a considerable cancellation since fields at the neighbouring nodes should not differ too much. Nevertheless, the above expression implies that the new term is quite important and ignoring it will lead to the first-order error in the interpolated field.

2.4 Numerical examples

We present results showing the effect of interpolation in two extreme cases of marine CSEM: infinite water depth and shallow water. In Fig. 3, we show how the interpolation error depends on the grid cell size for an infinite water depth. We choose the simplest possible CSEM example: a half-space water and half-space formation with resistivities of 0.3125 and 1 Ωm, respectively. The source is a harmonic horizontal electric dipole with dipole moment of 1 Am at the frequency of 1 Hz placed slightly above the seafloor. The inline electric field E_x at the seafloor has been computed using 3-D finite-difference time-domain code described by Maaø (2007) and Mittet (2010), and then compared to the semi-analytical solution, E_x^{true}, given in Løseth & Ursin (2007). The error of the 3-D code is characterized by the relative difference, $|E_x - E_x^{\text{true}}|/|E_x^{\text{true}}|$, (that includes both amplitude and phase information) averaged over source–receiver offsets from 3 to 10 km. The error is plotted in Fig. 3 as a function of the Yee cell size Δz, while the cell sizes in x and y are always 50 m. We can see that for the linear interpolation scheme (blue line) the error is first order, that is, proportional to Δz. This is in agreement with eq. (12) where the term proportional to Δz appears due to derivative discontinuity at the interface and is ignored in the linear interpolation. It also follows graphically from Fig. 1 that ignoring the sharp bend of the field profile leads to an error proportional to Δz. The proposed interpolation scheme (red line in Fig. 3) removes essentially all the interpolation error. The remaining error is much smaller and does not show a linear trend. It is mostly caused by the error of differential operators close to the seafloor. The error is not that large because we have performed proper averaging of water and formation conductivities for the grid nodes located at the seafloor (harmonic averaging for σ_z and arithmetic averaging for σ_x, σ_y). Nevertheless, the same derivative jump at the seafloor that creates the interpolation error, also creates a (smaller) error in the differential operators. For data shown in Fig. 3

Figure 4. Errors in the electric and magnetic fields recorded at the seafloor for various positions of the seafloor relative to the grid nodes. The conventional linear interpolation (blue) delivers large errors except for special cases when the recording position coincides with the corresponding node. The proposed rigorous interpolation (red) reduces the error dramatically and makes it essentially independent of the seafloor position.

we used differential operators of half-length 1 in z and half-length 2 in x and y.

Fig. 3 considers the case when the interface falls exactly in the middle between the layers of E_x nodes. This is the worst case scenario for linear interpolation scheme leading to the maximal interpolation error in E_x. The ideal case is when positions of E_x nodes coincide with the interface, then there is no need to interpolate E_x along the vertical direction, and the corresponding interpolation error is zero. Unfortunately, it is not possible to place all E_x nodes exactly at the seafloor in the general case of varying bathymetry (unless one uses unstructured grids). Moreover, even if all E_x and E_y nodes lie exactly at the seafloor, then the nearest H_x, H_y and E_z nodes of the staggered Yee grid will be located half a cell above and below it. Hence, one will have to interpolate H_x, H_y and E_z across the interface and deal with discontinuities of their derivatives given by eqs (4) and (5).

Fig. 4 displays errors in both E_x and H_y for various positions of seafloor relative to the Yee grid. They are computed for the same CSEM example as in Fig. 3, using 100 m cell size in z. If the interface falls in the middle between E_x nodes—the case considered in Fig. 3—then the linear interpolation error in E_x is maximal. At the same time, H_y nodes lie exactly at the interface, hence the error in H_y is small and independent of the interpolation scheme. The opposite situation is observed when the interface coincides with the plane of E_x nodes: then the maximal error is observed for the H_y component: up to 7 per cent for the linear interpolation that disregards derivative jumps. Obviously, for any position of interface relative to the Yee grid, taking into account the derivative discontinuities helps significantly reduce the error either for E_x, or for H_y, or for both of them. Note that with the new interpolation scheme the error becomes almost independent of the position of interface (where we record the fields) relative to the Yee cell. It implies that the new rigorous interpolation essentially removes all the errors related to the presence of interface.

Use of the proposed rigorous interpolation becomes especially important in the challenging case of very shallow water. To illustrate this we consider another CSEM problem, similar to that used in Fig. 1, but now the water layer is only 100 m thick (see Fig. 5). Moreover, the cell size in the vertical direction is also 100 m, which means that the water is represented by only one layer of cells. Let
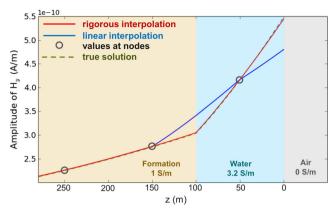
Figure 5. Magnitude of magnetic field as a function of the vertical coordinate z for a CSEM model with 100-m-thick water layer. Circles indicate field values computed at the nodes of modelling grid, while the lines are the interpolation results. Even though there is only one node in the water, the proposed rigorous interpolation reproduces very accurately the true field profile, in particular, its bend at the formation–water interface. The linear interpolation is obviously much less accurate.

us analyse the magnetic field now. It is directed along the y-axis in the inline configuration. There is only one layer of H_y nodes in the water, they are located in the middle of Yee cells, at a 50 m depth. In that case performing an accurate interpolation in the vertical direction is very challenging. Interpolation using only nodes in water is hardly possible since there is only one node available. Linear interpolation using one node in water and one in formation produces significant errors at the seafloor, as evident from Fig. 5. By contrast, the proposed rigorous interpolation is able to fit the true field profile very accurately because it 'knows' about the jump of field derivative at the seafloor and explicitly computes it using the known conductivity values on the both sides of interface. As a result, it arrives at the correct slope of field profile in the water, which makes the interpolation error at any location within the water layer remarkably small for a one-node interpolation problem. Good accuracy of the results for a shallow water model also demonstrates that our finite-difference approach is able to accurately handle a boundary with highly resistive air in the close vicinity to sources and receivers.
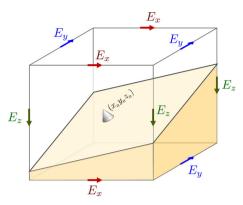
3 TILTED INTERFACE

In this section, we describe how one can interpolate EM fields across an interface that has an arbitrary orientation with respect to the modelling grid (see Fig. 6). First, in Section 3.1, we present a basic framework which takes into account discontinuity of the normal electric field only. Then, in Section 3.2 we show how discontinuities of the derivatives of tangential fields can be incorporated in the presented framework.

The interpolation needs to be carried out in the coordinate system aligned with the interface with subsequent transformation into the coordinate system (x, y, z) of the modelling grid. As a result, it is no longer possible to find interpolation coefficients separately for x, y and z, and compose the 3-D interpolation coefficients by simple multiplication, as in eq. (6). Instead, one has to set up the whole interpolation in 3-D.

3.1 Framework

The first step in our approach is to evaluate the orientation of interface close to the interpolation point. It is assumed that over a

Figure 6. Interface tilted with respect to the Yee grid. The goal of interpolation is to compute electric fields components at the recording location (x_0, y_0, z_0) from the known values of E_x, E_y and E_z at the grid nodes with a proper account of all boundary conditions at the interface.

distance of a few cells close to receiver the interface can be accurately approximated by a plane, that is, its curvature will be ignored. Let the angles θ and ϕ define the transform between the coordinate system (x, y, z) of the modelling grid and the new coordinate system (τ_x, τ_y, n) aligned with the interface. Namely, the new system is obtained by rotation by angle ϕ around the z-axis and then rotation by angle θ around the τ_x-axis. The third rotation around the normal n is not needed since the direction of axes τ_x and τ_y within the seafloor plane can be chosen arbitrarily. Thus the rotation matrix for converting a vector from (τ_x, τ_y, n) to (x, y, z) reads:

$$R = \begin{pmatrix} \cos\phi & -\sin\phi\cos\theta & \sin\phi\sin\theta \\ \sin\phi & \cos\phi\cos\theta & -\cos\phi\sin\theta \\ 0 & \sin\theta & \cos\theta \end{pmatrix}. \tag{14}$$

The interpolation problem for electric field at the recording side is formulated as follows: we know field values at all grid nodes corresponding to all components (E_x, E_y, E_z), and we need to find E_x, E_y and E_z at a specific recording location (x_0, y_0, z_0), see Fig. 6. So, the goal is to find the interpolation coefficients for every node and for every recorded field component. Due to presence of a tilted interface, there will appear all kind of crossed interpolation coefficients, hence to record any component, for example E_y, we will need to use values at all types of nodes: E_x, E_y and E_z. The problem at the source side is solved using the same interpolation coefficients, as explained in Section 4.

To describe the electric field vector it's convenient to use only quantities which are continuous over the interface, that is, the tangential fields $E_{\tau x}$, $E_{\tau y}$ and the normal current density J_n. In the vicinity of receiver, we approximate all of them using a Taylor expansion up to the first derivatives, for example, for $E_{\tau x}$ one obtains:

$$E_{\tau x}(\tau_x, \tau_y, n) = E_{\tau x0} + \frac{\partial E_{\tau x}}{\partial \tau_x}(\tau_x - \tau_{x0})$$

$$+ \frac{\partial E_{\tau x}}{\partial \tau_y}(\tau_y - \tau_{y0}) + \frac{\partial E_{\tau x}}{\partial n}(n - n_0). \tag{15}$$

Here $(\tau_{x0}, \tau_{y0}, n_0)$ is the receiver position in the coordinate system aligned with the interface.

There are four unknowns in the above equation: $E_{\tau x0}$ and the three derivatives. Combined with similar expansions for $E_{\tau y}$ and J_n, we end up with 12 unknowns. In order to find them, it would be sufficient to use known electric field values at 12 nodes of the modelling grid located close to the receiver. However, it is not clear which 12 nodes should be chosen and whatever choice is made, they will be distributed quite asymmetrically with respect to the

receiver position. It would be preferable to use nodes surrounding the receiver from both sides in each of three directions, leading to at least $2 \times 2 \times 2 = 8$ nodes for each field component. For E_x, E_y and E_z it gives 24 nodes in total, and hence an overdetermined system: 24 equations and only 12 unknowns. One can also use higher-order Taylor expansions instead of eq. (15), which leads to larger number of unknowns. Then one may need to include more nodes into the interpolation stencil: if there are M unknowns and N selected nodes then it is required that $M \leq N$.

For overdetermined systems the unknowns can be found by performing the least-squares fit of field values at the selected nodes, that is, by minimizing the functional,

$$S = \sum_{i=1}^{N} w_i \left[(E_\alpha(\mathbf{r_i}) - E_{\alpha i} \right]^2 . \tag{16}$$

The sum here is over the selected nodes where $\alpha = x, y, z$ depending on which node it is: E_x, E_y or E_z. Coefficients w_i are the weights that will be discussed in detail later. Then, $E_{\alpha i}$ is the known value at the node i, while r_i is position of that node in the (x, y, z) coordinate system, and $E_\alpha(\mathbf{r_i})$ is the electric field there evaluated from the Taylor expansions. More specifically, one needs to use the expansion of eq. (15) and similar ones for $E_{\tau y}$ and J_n at the node position and then perform a transform from quantities $E_{\tau x}$, $E_{\tau y}$, J_n evaluated at node i to E_{xi}, E_{yi}, E_{zi} at the same node i using the rotation matrix R from eq. (14) and the equality $E_{ni} = J_{ni}/\sigma_{ni}$. The quantities $E_{\tau x}$, $E_{\tau y}$, J_n are never computed explicitly, but are just used for constructing the system of equations that relates the field at the receiver location to the field in the staggered modelling grid.

It is easy to see that one can express $E_\alpha(\mathbf{r_i})$ as

$$E_\alpha(\mathbf{r_i}) = \sum_m e_{im} u_m, \tag{17}$$

where the sum is over all the unknowns ($E_{\tau x0}$, $E_{\tau y0}$, J_{n0}, and the corresponding derivatives) that are now denoted as u_m, $m = 1, \ldots, M$. Coefficients e_{im} depend on the coefficients in the Taylor expansions, rotation matrix R and values of σ_{ni}. Note that σ_i denotes here the effective conductivity for node i which is used in the finite-difference scheme and typically computed by proper averaging of conductivities in the volume around this node. Presence of a tilted interface implies that the effective conductivity tensor σ_i has non-zero off-diagonal elements even if the original two media are characterized by a diagonal conductivity tensor $\sigma(x, y, z)$. However, we shall assume that tensor σ_i is diagonal in the coordinate system aligned with the interface, and σ_{ni} is its principal value in the normal direction.

To minimize S one should set to zero the derivatives of S with respect to all unknowns, $\partial S / \partial u_m = 0$. This gives us a set of linear equations that can be written in the matrix form as

$$A\,U = b, \tag{18}$$

where $U = (u_1, \ldots, u_M)^T$ is the vector of unknowns, while the elements of the square matrix A are:

$$A_{mk} = \sum_{i=1}^{N} w_i \, e_{im} e_{ik}. \tag{19}$$

The right-hand side b can be expressed as

$$b = BF, \tag{20}$$

where $F = (E_{\alpha 1}, \ldots, E_{\alpha N})^T$ is a vector of field values at the N selected nodes (that include E_x, E_y and E_z nodes), while elements of matrix B are

$$B_{mi} = w_i e_{im}. \tag{21}$$

These definitions allow us to express the unknowns in a compact form,

$$U = (A^{-1}B)F. \tag{22}$$

The matrix product $(A^{-1}B)$ thus can give us all the interpolation coefficients. For interpolation one needs only three unknowns, $E_{\tau x0}$, $E_{\tau y0}$, J_{n0}, hence, only the three corresponding rows of matrix $(A^{-1}B)$ will be used. Finally, one needs to go from the quantities $E_{\tau x0}$, $E_{\tau y0}$, J_{n0}, to the corresponding values of E_x, E_y and E_z defined at the same location (location of receiver). For that purpose one should first divide J_{n0} by conductivity σ_n at the receiver location to get E_{n0}, and then transform the electric field vector $\mathbf{E}$ to the (x, y, z) coordinate system using eq. (14) for the rotation matrix R.

The other rows of the matrix $(A^{-1}B)$ correspond to spatial derivatives of $E_{\tau x}$, $E_{\tau y}$, J_n. The presented framework thus can be used not only to solve the interpolation problem, but also to build the finite-difference scheme in the presence of interfaces. Indeed, it allows one to evaluate all the field derivatives entering the Maxwell equations at desired locations close to sharp conductivity contrasts. Presentation of a framework that covers both the interpolation and differential operators will be given elsewhere. A similar framework for handling tilted interfaces was recently developed to compute differential operators (Bauer *et al.* 2011). One important difference from our approach is that Bauer *et al.* uses only four nearest nodes for the interpolation stencil, which is just enough to find all the unknowns.

The system of equations eq. (18) can be supplemented with additional conditions, if necessary. For example, if a CSEM survey is acquired in very shallow water using a surface-towed source (Barker *et al.* 2012) that is located at a few-metre depth, then the interpolation needs to be performed close to the sea surface. Let us now assume that the air is excluded from the computation domain, as was done, for example in Wang & Hohmann (1993) and Mittet (2010). Then, a boundary condition $E_z = 0$ must be satisfied at the sea surface since no currents can flow into the air. Including this boundary condition into the interpolation scheme should improve its accuracy. This can be done within the present framework by adding a few fictitious E_z nodes located at the sea surface at arbitrary (x, y) coordinates close to the interpolation site. These extra nodes should be included in the derivation starting with eq. (16) on equal grounds with other nodes. Eventually, the interpolation coefficients computed for these extra nodes should be disregarded because E_z was set to zero there. However, interpolation coefficients for all 'real' nodes will be modified due to including these fictitious nodes, so that the interpolated fields are in agreement with the imposed boundary conditions. Implementation of this supplementary boundary condition has been tested on the shallow-water CSEM example used for Fig. 5. Four fictitious E_z nodes were introduced at the air interface at the same (x, y) coordinates as regular E_z nodes of the grid. It allowed us to reduce the relative E_z error averaged over a depth interval of 50 m just below the sea surface from 1.6 to 1.0 per cent (the error was normalized to $|E_z^{\text{true}}|$ taken at the seafloor).

3.2 Derivative jumps

The presented framework allows one to avoid the problem with discontinuity of the normal electric field, E_n, because the interpolation is instead built on the continuous normal current density J_n. Now we need to take into account also discontinuities in the derivatives. For all the interpolated quantities, J_n as well as the tangential field components $E_{\tau x}$, $E_{\tau y}$, their normal derivative $\partial / \partial n$ has a jump

across the interface. Expressions for the jumps are given in Section 2.1 for an interface parallel to the (x, y) plane and normal in the z direction. Here we shall use the same expressions, but rewritten for an interface in the plane (τ_x, τ_y) and normal n.

The presence of derivative jumps requires that the Taylor expansion (15) is modified since the derivative $\partial E_{\tau x}/\partial n$ acquires different values at the two sides of the interface. One can write

$$\frac{\partial E_{\tau x}}{\partial n}(n - n_0)$$

$$= \begin{cases} \dfrac{\partial E_{\tau x1}}{\partial n}(n - n_0), & n \in \Omega_1, \\ \dfrac{\partial E_{\tau x1}}{\partial n}(n - n_0) + \left(\dfrac{1}{\sigma_{n2}} - \dfrac{1}{\sigma_{n1}}\right)\dfrac{\partial J_n}{\partial \tau_x}(n - n^*), & n \in \Omega_2, \end{cases}$$

$$(23)$$

where it is assumed that the receiver is located in medium Ω_1. A similar modification needs to be done to the term with $\partial E_{\tau y}/\partial n$. The jump in the derivative of the normal current is given by a rewritten eq. (5) as $\sigma_{n2}(\partial J_{n1}/\partial n) = \sigma_{n1}(\partial J_{n2}/\partial n)$. Thus term in the Taylor expansion for J_n will be modified to:

$$\frac{\partial J_n}{\partial n}(n - n_0) = \begin{cases} \dfrac{\partial J_{n1}}{\partial n}(n - n_0), & n \in \Omega_1 \\ \dfrac{\partial J_{n1}}{\partial n}\left[(n^* - n_0) + \dfrac{\sigma_{n2}}{\sigma_{n1}}(n - n^*)\right], & n \in \Omega_2. \end{cases}$$

$$(24)$$

The effect of these derivative jumps is that coefficients e_{im} in eq. (17) will be modified. For example, the result of jump in $\partial E_{\tau x}/\partial n$ is that coefficients e_{im_1} responsible for the unknown $\partial J_n/\partial \tau_x$ will get an additional term proportional to the resistivity jump, $(1/\sigma_{n2} - 1/\sigma_{n1})$, and to the coefficients e_{im_2} responsible for the unknown $\partial E_{\tau x1}/\partial n$. As a results, there will be changes in the matrices A and B defined by eqs (19) and (21), and one will eventually arrive at different values of the interpolation coefficients.

3.3 Weights

Let us now discuss coefficients w_i in eq. (16) that define relative weights of different grid nodes in the functional S to be minimized. In principle, one can simply set $w_i = 1$ for all nodes in the interpolation stencil, which gives reasonably good results. However, a somewhat problematic issue appears here if a receiver is located exactly at the grid node. One then normally expects that the interpolated value should coincide with the value at this node. This intuitive property is shared by most interpolation schemes, but it is not guaranteed in an overdetermined scheme. Indeed, in our scheme the number of unknowns is smaller than the number of nodes, hence the values at the nodes will be fitted in the best possible least-squares way, but not exactly.

This problem can be solved by setting weights inversely proportional to the distance between the node and the receiver,

$$w_i \propto |\mathbf{r_i} - \mathbf{r_0}|^{-1}.$$

$$(25)$$

Then for receiver close to a particular node, the weight of that node will be overwhelmingly high compared to weights of all other nodes. Minimization of S will then produce a function that acquires the specified values at all the nodes and smoothly interpolates in between.

The same result can be achieved if the weights are set to depend separately on the distances along the three coordinates:

$$w_i \propto |(x_i - x_0)(y_i - y_0)(z_i - z_0)|^{-\gamma}$$

$$(26)$$

rather than on the 3-D distance as in eq. (25). The exponent γ can take any positive value, we used $\gamma = 0.5$, and also avoided the divergence by introducing a cut-off at small distances ~ 1 m. The advantage of this scheme shows up when a receiver aligns with positions of grid nodes along one of the coordinates. Let us assume, for example that the x coordinate of receiver, x_0, coincides with the x coordinate of one layer of E_x nodes. Then intuitively one expects that only E_x nodes with $x_i = x_0$ should be used for interpolation of component E_x at the receiver, while interpolation coefficients for nodes beyond the plane $x = x_0$ must be zero. The present weighting scheme guarantees exactly that. Its additional advantage is that the interpolation coefficients always change continuously when the receiver is moved across the grid. Even small changes in the receiver position may change the interpolation stencil that covers the nearest 24 nodes, however the continuity is still preserved because the interpolation coefficients for the most distant nodes in the stencil are always zero. Our interpolation scheme thus preserves the continuity of the recorded field components everywhere within the grid, but accurately reproduces discontinuities across the interface even though it may cross the grid at an arbitrary position and at an arbitrary angle.
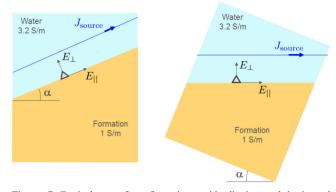
Finally, let us discuss a small modification of weights that helps balance the contributions of E_z nodes on both sides of the interface. Since the seafloor is usually more or less horizontal, a jump of normal electric field at the seafloor results in much lower values of E_z in the water than in formation. All terms in the minimization functional (16) are proportional to the field squared, therefore E_z nodes in formation will normally have a much stronger effect on the interpolated value at the receiver than E_z nodes in water. To compensate for this asymmetry, one can multiply the weights in eq. (16) by σ_{zi}^2, where σ_i denotes the effective conductivity for node i. This factor will ensure that E_z nodes in water and in formation located at the same distance from the receiver will have equal effect on the interpolated value (for a horizontal seafloor).

3.4 Numerical example

3.4.1 Model description

The accuracy of the proposed interpolation scheme for a tilted interface has been tested on a marine CSEM example where the seafloor is dipping. The seafloor represented a sharp conductivity contrast between the water conductivity above, 3.2 S m^{-1} and formation conductivity below, 1 S m^{-1}. The dip angle of the seafloor was $20°$. The strike direction was at an angle of $30°$ with the respect to the x-axis, which is essentially the case shown in Fig. 6. Hence, we considered the most general orientation of the seafloor with respect to the finite-difference grid.

The receiver was located exactly at the seafloor, while the electric dipole source was towed 30 m above it. In the first run, the cell sizes of the grid were relatively coarse $200 \times 200 \times 50$ m in x, y and z, respectively. These sizes are quite practical when working with EM data coming from today's large-scale full-azimuth 3-D surveys, if one aims at realistic times for the full 3-D inversion of survey data. It is therefore important to know whether a finite-difference scheme can handle large dip angles with acceptable accuracy for these coarse cell sizes. Note that the CSEM source is located approximately

Figure 7. Equivalence of configurations with dipping and horizontal seafloors: electric field *E* measured by receiver will be the same in both configurations provided water and formation occupy half-spaces. Hence, the exact solution available for the horizontal seafloor can be used for the dipping floor case after proper coordinate transformation. In the presented numerical example the dip angle, α, was 20°.

half a cell above the seafloor, hence interpolation for many source positions included not only nodes in the water, but also nodes in the formation. Thus in the present example the interpolation is carried out across the seafloor both for the source position and for the receiver. The computations were performed with a finite-difference time-domain 3-D code described by Maaø (2007) and Mittet (2010).

In order to evaluate the accuracy of 3-D modelling code, its results should be compared to the exact solution for the considered dipping-floor model. Despite the semi-analytical solution for the CSEM problem (Løseth & Ursin 2007) is available only for horizontally layered earth, it is possible to use it for a dipping floor too, as illustrated in Fig. 7. The trick here is to rotate the coordinate system so that the seafloor becomes horizontal. The computed fields in both configurations will be equivalent if the water and formation layers

are infinitely deep. To make sure that these conditions are fulfilled, the 3-D modelling was based on a resistivity model with very deep water layer: the model dimensions were $24 \times 24 \times 30$ km, and the water depth varied from 4 km in the shallowest to ≈ 16 km in the deepest part.

The source was towed along the dip direction parallel to the seafloor and the source dipole was pointing in the same direction, that is had a pitch of 20° (see Fig. 7, left-hand panel). Due to the symmetry of the problem, the electric field at the receiver location lies in the dipping plane—the plane shown in the figure. We shall analyse separately the field component recorded parallel to the seafloor, $E_{||}$, and its component normal to the seafloor, $E_\perp$.

3.4.2 Results

Let us compare three interpolation schemes:

(i) *Rigorous interpolation*—the interpolation method proposed in this paper based on equations in Sections 3.1 and 3.2.

(ii) *Rigorous interpolation without derivative jumps*—the same method, but without taking into account the jumps of field derivatives at the interface. In other words, we use the framework of Section 3.1 that accounts for discontinuity of the normal field E_n, but disregard discontinuity of $\partial E_{\tau x}/\partial n$, $\partial E_{\tau y}/\partial n$ and $\partial J_n/\partial n$ described in Section 3.2.

(iii) *Trilinear interpolation in the water*—the standard trilinear interpolation, but using only grid nodes located within the water layer to avoid issues with discontinuities at the seafloor. The interpolation will first try to use the $2 \times 2 \times 2 = 8$ nearest nodes, but if at least one of them falls below the seafloor, it will instead use another set of eight nodes obtained by moving one cell up to make sure all the eight nodes are in the water (sometimes one may need to move up by two or more cells).
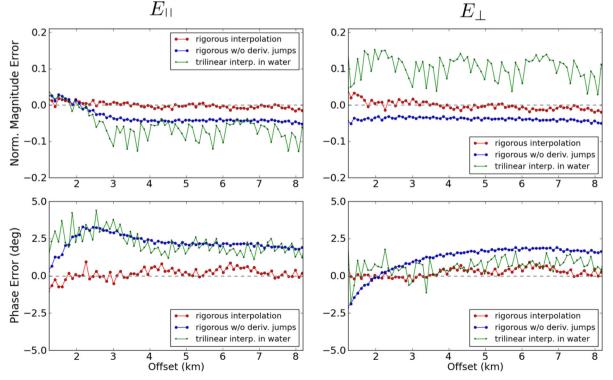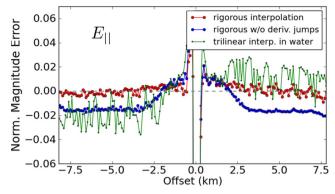
Figure 8. Magnitude and phase error for different interpolation schemes for electric field components $E_{||}$ parallel and $E_\perp$ normal to the seafloor that is tilted by 20 degrees relative to the modelling grid. The proposed rigorous interpolation gives the best results at essentially all source–receiver offsets. Frequency 0.25 Hz.

Figure 9. Normalized magnitude error for different interpolation schemes on a finer grid ($100 \times 100 \times 25$ m) than in Fig. 8. Shown is the electric field $E_{||}$ parallel to the seafloor that is dipping at $20°$, the frequency is 0.25 Hz. The error is asymmetric in the downdip and updip directions, but in both directions the rigorous interpolation proposed in the paper is the most accurate.

Fig. 8 displays the error in the electric field E computed by the 3-D code using different interpolation schemes, as compared to the exact solution E^{true} of Løseth & Ursin (2007) after rotating the coordinate system. Shown at the top row is the error in the normalized magnitude $|E/E^{\text{true}}| - 1$, while the bottom row shows the difference in phases for E and E^{true}. The left-hand plots correspond to the component $E_{||}$ parallel to the seafloor, while the right plots—to the normal field, $E_\perp$. The proposed rigorous interpolation (red curve) clearly gives the best results on all the four plots. Ignoring the discontinuity of derivatives at the interface (blue curve) leads to a systematic error both in magnitude and in phase. The magnitude is again underestimated, like in the case with a horizontal seafloor in Fig. 1. Interpolation using nodes in the water only (green curve) also leads to a systematic error and in addition results in chaotic oscillations from point to point. Small oscillations are also present at the two other curves because the interpolation accuracy is affected by the relative position of interpolation location with respect to the grid nodes. This effect however becomes much stronger for the interpolation scheme using only nodes in water since they are in general farther away from the interpolation point.

Shown in Fig. 9 are similar results for the parallel field, $E_{||}$, obtained on a finer grid, $100 \times 100 \times 25$ m, that is with halved cell sizes in all directions. Smaller cell sizes naturally lead to smaller errors for all interpolation methods, however the proposed rigorous interpolation still provides the best results. This figure shows both intow and outtow offsets in order to illustrate that the interpolation

error can be very asymmetric in the downdip and updip directions—this is clearly the case for the green curve (trilinear interpolation using water nodes).
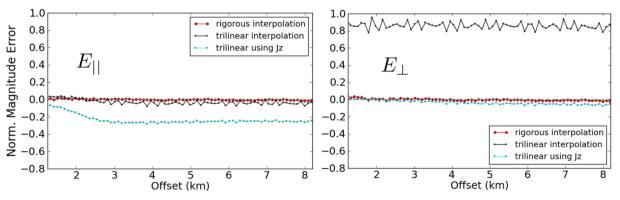
3.4.3 Naive interpolations

In addition to the three interpolation methods compared in Figs 8 and 9, we would like to consider also two 'naive' interpolation approaches and explain why they fail in the presence of tilted interfaces. These approaches are:

(iv) *Trilinear interpolation*—in its simplest form where it is based on the $2 \times 2 \times 2 = 8$ nearest nodes even if they are located at different sides of the interface. The interpolated quantities are E_x, E_y and E_z.

(v) *Trilinear interpolation using J_z*—a modification of trilinear interpolation that makes use of the fact that the seafloor is often nearly horizontal. Instead of interpolating the vertical electric field E_z that has a clear jump at the seafloor, one here interpolates the vertical current density J_z. This approach is very accurate in the case of horizontal seafloor where J_z is continuous indeed. Therefore one may expect that for small dipping angles, J_z is still a much smoother function than E_z and hence hope for relatively small interpolation errors.

The results for both interpolation methods are presented in Fig. 10 as plots of the normalized magnitude error versus offset for the same model and parameters as in Fig. 8. Note that the scale of y-axis now is different because both naive interpolations are very inaccurate when the dipping angle is 20 degrees. The standard trilinear interpolation works reasonably well only for the field component $E_{||}$ that is parallel to seafloor and therefore exhibits a smooth behaviour (top panel). The error for the normal component, $E_\perp$, is however huge (bottom panel) because its values in formation are much larger than those in water and this fact is disregarded. Trilinear interpolation using J_z provides a much better accuracy for $E_\perp$ since it respects the fact that the vertical field $E_z = J_z/\sigma_z$ has larger values in the formation. Small misalignment between $E_\perp$ and E_z does not lead to significant errors in this case. However, this interpolation method becomes very inaccurate for the component $E_{||}$ parallel to the seafloor, see the top panel again. The field $E_{||}$ is continuous across the seafloor, and discontinuity of E_z which is imposed in this method, leads to significant discontinuous component in $E_{||}$ resulting in large interpolation errors.

We listed average errors for all the interpolation schemes in Table 1. In order to include both amplitude and phase errors, we

Figure 10. Normalized magnitude error for the rigorous interpolation (red) and two naive interpolation schemes. Trilinear interpolation using the vertical current density J_z gives very large errors in the electric field $E_{||}$ parallel to the dipping seafloor (top panel), while the standard trilinear interpolation leads to huge errors in the normal electric field, $E_\perp$ (bottom panel). The dipping angle is 20 degrees, frequency is 0.25 Hz and the cell sizes are $200 \times 200 \times 50$ m.

Table 1. Averaged errors (in per cent) in electric field for several interpolation methods.

Cell sizes		200 × 200 × 50 m				100 × 100 × 25 m			
Field component		$E_{\|\|}$		$E_\perp$		$E_{\|\|}$		$E_\perp$	
Frequency		0.25 Hz	1 Hz	0.25 Hz	1 Hz	0.25 Hz	1 Hz	0.25 Hz	1 Hz
(i)	Rigorous interpolation	1.3	3.0	1.6	3.0	0.8	1.6	1.2	2.3
(ii)	Rigorous interpolation w/o derivative jumps	5.1	8.9	4.4	8.3	2.4	4.7	2.1	4.5
(iii)	Trilinear interpolation using nodes in water	6.1	10.2	18.1	18.8	4.2	5.4	17.8	17.3
(iv)	Trilinear interpolation	6.2	9.9	54.7	53.1	3.5	5.4	55.6	54.7
(v)	Trilinear interpolation using J_z	20.7	26.2	7.5	9.5	21.4	22.9	14.4	14.0

again used the quantity $|E - E^{\text{true}}|/|E^{\text{true}}|$. Root mean square average of this quantity was computed over the range of source–receiver offsets from 1.5 to 8 km including both the downdip and updip directions. At shorter offsets there appears significant error due to discretization of the point source, while at very long offsets boundary effects become noticeable. However in the chosen interval of intermediate offsets the total computational error is dominated by the error of interpolation scheme. The rigorous interpolation proposed in this paper demonstrates the best accuracy for all the field components, frequencies and cell sizes included in the analysis.
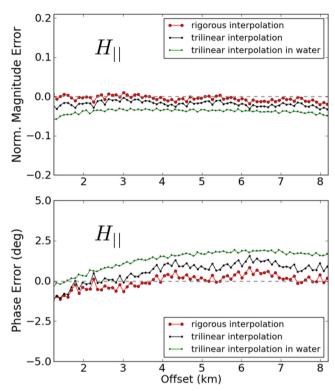
3.4.4 Magnetic field

The proposed rigorous interpolation taking into account the derivative jumps at the interface can be applied not only for the electric fields, as demonstrated in Sections 3.1–3.3, but also for the magnetic fields. We consider interfaces characterized by a jump in the electric conductivity, while the magnetic permeability is assumed uniform. Such interfaces are in general a smaller problem for the magnetic field since all its components remain continuous (unlike the normal E that has a jump), and one of them—the normal H—even has a continuous derivative. Thus, the interpolation errors for magnetic fields are usually smaller and even a tilted interface would never lead to catastrophic errors of the kind displayed in Fig. 10 for the electric fields.

The above considerations are confirmed by Fig. 11 showing the magnitude and phase errors for the tangential magnetic field $H_{\|}$ for the same CSEM model with a 20° dipping seafloor as was used for Fig. 8. In this inline configuration the magnetic field at the receiver is directed normal to the plane depicted in Fig. 7. The normal magnetic field $H_\perp$ is not shown on the plot not so much because it is zero, but more importantly because its derivative is continuous over the seafloor and therefore all interpolation approaches give equally good results for $H_\perp$. Errors in the tangential H shown in Fig. 11 are smaller than those in E in Fig. 8. Even for a simple trilinear interpolation (black) they hardly exceed 2 per cent. Trilinear interpolation using nodes in the water (green) gives here a larger error because the interpolation stencil is further away from the recording position. At the same time, interpolation that takes into account the derivative discontinuity at the seafloor (red) again produces the smallest error. Interpolation for the electric source towed 30 m above the seafloor was in all these cases performed using the rigorous interpolation scheme for E field presented in Sections 3.1–3.3. Thus, the difference between the three curves in Fig. 11 stems solely from the interpolation method used for the magnetic field recorded at the seafloor.

4 DISCUSSION

The proposed rigorous interpolation is based on the properties of the Maxwell equations and therefore requires more input information

Figure 11. Normalized magnitude and phase errors for the tangential magnetic field. The smallest error is found for the proposed rigorous interpolation scheme (red). All parameters are the same as for Fig. 8 showing the electric field errors: 20° dip, frequency of 0.25 Hz, 200 × 200 × 50 m cell sizes.

than conventional interpolation schemes. In addition to the recording position relative to the grid nodes, one also needs to know (i) the position of interface, (ii) the interface normal and (iii) the conductivity values at each side of interface. With this information in place, one can explicitly compute the derivative jumps at the interface and hence safely interpolate using nodes on both sides of an interface.

The physics and necessary conditions to solve the problem is most easily understood in a 1-D setting, as shown in Section 2. An important property of the proposed rigorous interpolation is that it mixes different field components. For example, eq. (13) shows that evaluation of E_x at an arbitrary receiver location, may require not only values of E_x computed at the surrounding nodes, but also surrounding values of E_z. There is also mixing of magnetic and electric fields, for example it follows from eqs (4) that in order to interpolate H_x one needs not only H_x, but also E_y nodes. In the case of an interface misaligned with the grid, the mixing of field components is even more complex, as shown in Section 3.

We have presented a first-order rigorous interpolation, but the same framework can be also extended to higher orders. This can be done by using higher order Taylor expansions instead of

first-order expansions in eqs (7) and (15). Correspondingly, one will then need a longer interpolation stencil on both sides of the interface. Extending the analysis of Section 2.1 to higher-order derivatives shows that many of them are also discontinuous across an interface and those discontinuities should also be included into a higher-order interpolation scheme. Finally, we would like to mention that the proposed interpolation scheme will work for uniform, for non-uniform and even for unstructured grids.

The proposed interpolation can be applied not only at the recording positions, but also for the interpolation of EM source if its position doesn't coincide with a relevant grid node. The interpolation coefficients then tell how large weight of the source should be placed on every neighbouring node of the modelling grid. Luckily, due to the reciprocity property of the Maxwell equations, the interpolation coefficients are identical for the source and for receiver interpolation. Hence, one can use exactly the same strategy to derive the interpolation coefficients in both cases. Field components will get mixed also in the case of source interpolation, for example, to model an electric dipole source in the x-direction located at a horizontal interface, we should place some source terms at the surrounding E_x nodes and some small 'fictitious' source terms at the surrounding E_z nodes.

The error of several interpolation methods is quantified for two choices of modelling grid in Table 1. The poor results of conventional interpolation schemes come from the fact that the normal electric field is discontinuous at the interface, and this introduces discontinuities in the normal derivative of other field components. Hence, any interpolation method based on analytic functions across the interface will lead to an error proportional to the grid cell size. Table 1 suggests that without a proper account of the derivative discontinuities, one needs to reduce the cell size by at least a factor of 2 to achieve the same accuracy. Indeed, the best interpolation method neglecting the derivative jumps for a $200 \times 200 \times 50$ m grid leads to an error of 5.1 per cent for the tangential field $E_{\parallel}$ at 0.25 Hz. By using a finer grid $100 \times 100 \times 25$ m one can reduce the error significantly: to 2.4 per cent, at the expense of longer computational time. However one can keep the coarse grid, but apply the proposed interpolation scheme: the error will be reduced even more, down to 1.3 per cent, while the computational time would not change. For a time domain finite difference method halving the cell size translates to an increase in the computational time by at least a factor of $\sim 2\sqrt{2}$ (where we took a conservative approach that only cell size in vertical direction Δz matters and assumed that a time step is proportional to $\sqrt{\Delta z}$). Numerical example for a horizontal interface, Fig. 3, shows that the resulting increase in the computational time can be significantly larger.

It is important to take into account discontinuities at the seafloor only if the conductivity jump there is significant. Measurements performed using near-surface EMs in the Baltic Sea give conductivity for the bottom water layer of ~ 2.6 S m^{-1}, while conductivity of the top formation varies between 0.03 and 1.3 S m^{-1} (Müller *et al.* 2011). It means that the conductivity changes at the seafloor very abruptly by at least a factor of 2, and at some locations by more than a factor of 10. Thus, a conductivity jump of 3.2 assumed in our numerical examples is a fairly realistic number.

5 CONCLUSIONS

We present a rigorous interpolation method for finite difference EM modelling that can handle interfaces misaligned with the modelling grid. The method is based on properties of the Maxwell equations that dictate not only a discontinuity of the normal electric field at the interface, but also discontinuities of the derivatives of other field components. Taking into account the derivative discontinuity removes a first-order error of conventional interpolation schemes that are based on continuous analytic functions. The proposed method allows using a coarser grid close to interfaces that in our numerical examples reduces the computational time by a factor of ~ 3.

In the proposed method, the derivative jumps are computed explicitly by using conductivity values at each side of the interface. As a result, one can interpolate using grid nodes on both sides of the interface without any accuracy loss. The proposed interpolation mixes field components e.g. the interpolation stencil for E_x includes not only the nearest E_x nodes, but also nearest E_y and E_z nodes.

The interpolation can be fine-tuned using weighting scheme because it is based on solving an overdetermined system of equations. It also allows adding boundary conditions if a model boundary is located close to an interface. Finally, the proposed rigorous interpolation can be applied to both sources and receivers, can handle non-uniform and unstructured grids and can be used not only for an interface between two conductors, but also for an interface between two dielectrics.

REFERENCES

Abubakar, A., Habashy, T.M., Druskin, V.L., Knizhnerman, L. & Alumbaugh, D., 2008. 2.5D forward and inverse modeling for interpreting low-frequency electromagnetic measurements, *Geophysics*, **73**, F165–F177.

Alcocer, J.E., Garca, M.V., Soto, H.S., Baltar, D., Paramo, V.R., Gabrielsen, P. & Roth, F., 2013. Reducing uncertainty by integrating 3D CSEM in the mexican deep-water exploration workflow, *First Break*, **31**, 75–79.

Avdeev, D.B., 2005. Three-dimensional electromagnetic modelling and inversion from theory to application, *Surv. Geophys.*, **26**, 767–799.

Barker, N.D., Morten, J.P. & Shantsev, D.V., 2012. Optimizing em data acquisition for continental shelf exploration, *Leading Edge*, **31**(11), 1276–1284.

Bauer, C.A., Werner, G.R. & Cary, J.R., 2011. A second-order 3D electromagnetics algorithm for curved interfaces between anisotropic dielectrics on a Yee mesh, *J. Comput. Phys.*, **230**, 2060–2075.

Börner, R.-U., 2010. Numerical modelling in geo-electromagnetics: advances and challenges, *Surv. Geophys.*, **31**(2), 225–245.

Constable, S., 2010. Ten years of marine CSEM for hydrocarbon exploration, *Geophysics*, **75**(5), 75A67–75A81.

Hesthammer, J., Stefatos, A., Boulaenko, M., Fanavoll, S. & Danielsen, J., 2010. CSEM performance in light of well results, *Leading Edge*, **29**(1), 34–41.

Løseth, L. & Ursin, B., 2007. Electromagnetic fields in planarly layered anisotropic media, *Geophys. J. Intl.*, **170**, 44–80.

Maaø, F.A., 2007. Fast finite-difference time-domain modelling for marine-subsurface electromagnetic problems, *Geophysics*, **72**, 19–23.

Mittet, R., 2010. High-order finite-difference simulations of marine CSEM surveys using a correspondence principle for wave and diffusion fields, *Geophysics*, **75**, 33–50.

Morten, J., Roth, F., Karlsen, S., Timko, D., Pacurar, C., Olsen, P., Nguyen, A. & Gjengedal, J., 2012. Field appraisal and accurate resource estimation from 3D quantitative interpretation of seismic and CSEM data, *Leading Edge*, **31**(4), 447–456.

Müller, H., von Dobeneck, T., Nehmiz, W. & Hamer, K., 2011. Near-surface electromagnetic, rock magnetic, and geochemical fingerprinting of submarine freshwater seepage at Eckernförde Bay (SW Baltic Sea), *Geo-Mar. Lett.*, **31**(2), 123–140.

Nadobny, J., Sullivan, D., Wlodarczyk, W., Deuflhard, P. & Wust, P., 2003. A 3-D tensor FDTD-formulation for treatment of sloped interfaces in electrically inhomogeneous media, *Anten. Propagat., IEEE Trans.*, **51**(8), 1760–1770.

Roth, F., Lie, J., Panzner, M. & Gabrielsen, P., 2013. Improved target imaging with a high-power deck-mounted CSEM source—a field example from the North Sea, in *Proceedings of the 75th EAGE Conference & Exhibition*, pp. Tu 11 10.

Streich, R., 2009. 3D finite-difference frequency-domain modeling of controlled-source electromagnetic data: direct solution and optimization for high accuracy, *Geophysics*, **74**, F95–F105.

Taflove, A. & Hagness, S.G., 2005. *The Finite-Difference Time Domain Method*, Artech House.

Wang, T. & Hohmann, G., 1993. A finite-difference, time-domain solution for three-dimensional electromagnetic modeling, *Geophysics*, **58**, 797–809.

Wirianto, M., Mulder, W. & Slob, E., 2011. Applying essentially non-oscillatory interpolation to controlled-source electromagnetic modelling, *Geophys. Prospect.*, **59**, 161–175.